Design and Synthesis of the Beryllium–Free Deep–Ultraviolet Nonlinear Optical Material Ba3 (ZnB5 O10)PO4

ARTICLE *in* ADVANCED MATERIALS · OCTOBER 2015

Impact Factor: 17.49 · DOI: 10.1002/adma.201503951

5 AUTHORS, INCLUDING:

Hongwei Yu

University of Houston

93 PUBLICATIONS **606** CITATIONS

SEE PROFILE

Weiguo Zhang

University of Houston

25 PUBLICATIONS **341** CITATIONS

SEE PROFILE

Joshua Young

Drexel University

10 PUBLICATIONS **22** CITATIONS

SEE PROFILE

Shiv Halasyamani

University of Houston

266 PUBLICATIONS **5,665** CITATIONS

SEE PROFILE

Design and Synthesis of the Beryllium-Free Deep-Ultraviolet Nonlinear Optical Material $Ba_3(ZnB_5O_{10})PO_4$

Hongwei Yu, Weiguo Zhang, Joshua Young, James M. Rondinelli, and P. Shiv Halasyamani**

Nonlinear optical (NLO) materials are of intense interest owing to their ability to control and manipulate light for the generation of coherent radiation at a variety of difficult to access wavelengths. They have efficiently expanded the spectral ranges of solid state lasers from ultraviolet (UV) to infrared (IR).[1–5] Accessing directly the deep-ultraviolet (DUV) region (λ < 200 nm), however, is especially challenging,[6,7] yet vital to a number of advanced optical technologies, including photolithography for microelectronics and attosecond pulse generation for electron dynamic studies in matter.[4] Here, we report the design and synthesis of a chemically benign Be-free borate-phosphate, $Ba_3(ZnB_5O_{10})PO_4$ (BZBP), which exhibits a wide transparency range with second-harmonic-generating properties comparable to $KBe_2BO_3F_2$ (KBBF),[4] the only material capable of generating coherent DUV radiation directly using direct second harmonic generation (SHG). BZBP is air stable to 1000 °C and melts congruently, allowing for facile growth of large crystals and making it ideally suited for NLO applications in the DUV. Our strategy for NLO design will facilitate the discovery and expansion of next-generation optical crystals, enabling access to radiation at wavelengths throughout the electromagnetic spectrum.

For more than 50 years, the discovery and commercialization of many NLO materials, such as β-BaB_2O_4 (β-BBO), LiB_3O_5, $CsLiB_6O_{10}$, CsB_3O_5, $LiNbO_3$, $KTiOPO_4$, $AgGaQ_2$ (Q = S, Se), and $ZnGeP_2$ have been achieved.[3,4,8] Although these materials largely satisfy the frequency-conversion requirements from the UV to the IR, the direct generation of DUV coherent light by SHG has remained elusive. When possible, DUV radiation is achieved by a complex sum frequency method or using quasi-phase-matching approaches.[9] The complexity of direct light generation is attributable, in part, to poor birefringence, crystal quality and growth issues, as well as redshifted absorption edges in currently available materials.[3–5]

Dr. H. Yu, Dr. W. Zhang, Prof. P. S. Halasyamani
Department of Chemistry
University of Houston
112 Fleming Building, Houston, TX 77204-5003, USA
E-mail: psh@uh.edu
J. Young
Department of Materials Science and Engineering
Drexel University
3141 Chestnut Street, Philadelphia, PA 19104, USA
J. Young, Prof. J. M. Rondinelli
Department of Materials Science and Engineering
Northwestern University
2220 Campus Drive, Evanston, IL 60208-3108, USA
E-mail: jrondinelli@northwestern.edu

DOI: 10.1002/adma.201503951

A crucial requirement for DUV NLO materials design is a wide transparency window for the crystal, i.e., an absorption edge less than 200 nm (>6.2 eV). Considering this materials property criterion, researchers have mainly focused on beryllium borates, such as KBBF,[4] $SrBe_2B_2O_7$ (SBBO),[10] and $Na_3Sr_3Be_3B_3O_9F_4$ (NSBBF),[11] because the fundamental band gap for the borate is in the DUV. KBBF is the only borate able to frequency double light in the DUV through SHG; however, commercial applications of it are limited as its synthesis relies on carcinogenic BeO powders thus prohibitive precautions are required during crystal growth.[4,10–13] Growth of large single crystals is also difficult owing to its layered (lamellar) crystal habit. In order to circumvent the former problem, Be-free materials are greatly desired.

Recent research has shown that chemically benign phosphates may be optimal candidates for Be-free NLO materials that are operative in the DUV.[14–17] A series of non-centrosymmetric phosphates with short absorption edges, including $Ba_3P_3O_{10}X$ (X = Cl, Br) (180 nm for $Ba_3P_3O_{10}Cl$ and <200 nm for $Ba_3P_3O_{10}Br$),[14] $RbBa_2(PO_3)_5$ (163 nm),[15] $Rb_2Ba_3(P_2O_7)_2$ (<200 nm),[15] $Ba_5P_6O_{20}$ (167 nm),[16] and $CsLa(PO_3)_4$ (167 nm),[17] have been synthesized. However, the SHG responses of these phosphates range between (0.3–1.4) × KH_2PO_4 (KDP) and are not large enough for efficient frequency conversion.[5] Notably, the phosphate compound BPO_4 has a very short absorption edge (≈130 nm), in addition to a larger SHG response (2 × KDP).[18] Unfortunately, BPO_4 exhibits an extremely small birefringence, ≈0.005, in the visible region,[18] which makes conventional phase matching impossible and the material unusable for NLO. Nonetheless its optical absorption and SHG efficiency indicate that compounds containing both borate and phosphate units would be the ideal DUV NLO materials.

Materials containing both borate and phosphate anionic groups are classified into two categories: borophosphates and borate-phosphates.[19,20] The borate and phosphate groups are connected in borophosphates, such as BPO_4. In contrast, the anionic groups are not connected in borate-phosphates. It is thought that borate-phosphates are more advantageous for NLO applications than borophosphates, since the former contains BO_3 groups,[19–21] which have been shown to favor larger birefringence and SHG responses.[22] Last, the SHG response of borates can be enhanced by the addition of acentric ZnO_4 tetrahedra. These NLO-active building units achieve the desired response without shifting the absorption edge[23] owing to the fully filled d-orbitals of the Zn^{2+} cations.

By drawing upon these chemical insights, we designed ZnO_4 tetrahedra, PO_4 tetrahedra, and B–O groups into one compound and successfully synthesized the first DUV NLO zinco-borate-phosphate crystal, BZBP. This material has significant

advantages over KBBF, in that it does not require toxic BeO, does not exhibit the difficult to process layered structure, and melts congruently. The latter allows the growth of large single crystals. Our approach of combining multiple anionic groups in an acentric manner with a wide transparency range (>6.2 eV) offers a promising strategy toward the discovery of new optical materials with NLO functionalities in the UV and DUV.

Pure and polycrystalline BZBP was synthesized through solid-state techniques by combining stoichiometric amounts of $BaCO_3$, ZnO, H_3BO_3, and $NH_4H_2PO_4$ in a Pt crucible and heating in air (see the Experimental Section). The phase purity was confirmed by powder X-ray diffraction (Figure S1, Supporting Information). Single crystals of BZBP were grown by the top-seeded solution growth method. A H_3BO_3–ZnO flux system was used for the crystal growth. The mixture was placed in a Pt crucible and melted at 980 °C. This temperature was held for 15 h after which a Pt wire was dipped into the clear melt. Small crystals appeared on the Pt wire and were used as seed crystals. Using the seed crystals, BZBP crystals of $\approx 9 \times 7 \times 3$ mm^3 were grown and indexed (**Figure 1**a). Layering of the single crystal is not observed in BZBP, which overcomes the layering-growth habit along the *c*-axis reported for KBBF, attributable to the ZnB_5O_{10} units that are linked in three dimensions (see below). The differential thermal analysis (DTA) and thermogravimetric (TG) curves of BZBP are shown in Figure S2 (Supporting Information). There is only one endothermic (exothermic) peak on the heating (cooling) curve at 937 °C (827 °C), indicating BZBP melts congruently. In addition, there was no weight loss observed up to 1000 °C. Finally, a BZBP crystal was placed in water for a week with no decomposition or degradation observed (Figure S3, Supporting Information).

BZBP crystallizes in the noncentrosymmetric orthorhombic polar space group $Pmn2_1$ (Table S1, Supporting Information). In the asymmetric unit, there are two unique Ba atoms, one unique Zn atom, one unique P atom, three unique B atoms, and nine O atoms (Table S2, Supporting Information). The B atoms exhibit two types of coordination environments—BO_3 triangles and BO_4 tetrahedra. The B–O bond distances range from 1.330(8) to 1.396(9) Å and 1.463(7) to 1.491(7) Å, respectively. The P and Zn atoms are coordinated by four O atoms to form PO_4 and ZnO_4 tetrahedra. The P–O and Zn–O bond distances range from 1.539(4) to 1.545(6) Å and 1.941(7) to 2.065(6) Å, respectively. The Ba atoms are coordinated by nine O atoms with Ba–O bond lengths ranging from 2.549(7) to 2.938(5) Å (Table S3, Supporting Information). These bond lengths are consistent with those reported for oxides containing Ba, including known borophosphates.[24,25] The IR spectrum (Figure S4, Supporting Information) and the bond valence sums of each atom[26] (Table S2, Supporting Information) are also consistent with the assigned coordination environments and oxidation states.

The basic building unit of BZBP is a three six-membered ring $[ZnB_5O_{10}]$ group composed of three $[BO_3]$ triangles, two $[BO_4]$ tetrahedra, and one $[ZnO_4]$ tetrahedron that are corner-shared through oxygen atoms (Figure 1b). Adjacent $[ZnB_5O_{10}]$ building units share corners to create a $[ZnB_5O_{10}]_\infty$ framework (Figure 1c). The Ba atoms and the isolated PO_4 tetrahedra fill the spaces of the $[ZnB_5O_{10}]_\infty$ framework (Figure 1d). These crystal structure features make BZBP a zincoborate-phosphate as defined earlier.

Polycrystalline BZBP has a large transmission, >90%, from 230 to 2500 nm, with a short UV cutoff edge below 200 nm as determined from the UV–vis–IR diffuse-reflectance spectrum (**Figure 2**a). In fact, the reflectance at 200 nm is nearly 80%, indicating BZBP is transparent well below 200 nm. In order to investigate the DUV absorption, additional measurements were performed on a single crystal of BZBP on a McPherson VUVas2000 spectrophotometer from 120 to 350 nm. Figure 2b indicates that the absorption edge is 180 nm, confirming that the optical transparency of BZBP is advantageous for frequency generation in the DUV.

We next examine the frequency doubling capabilities of polar BZBP. Powder SHG measurements were performed with incident radiation at 1064 and 532 nm following the method described in ref. [27]. Following illumination, frequency-doubled

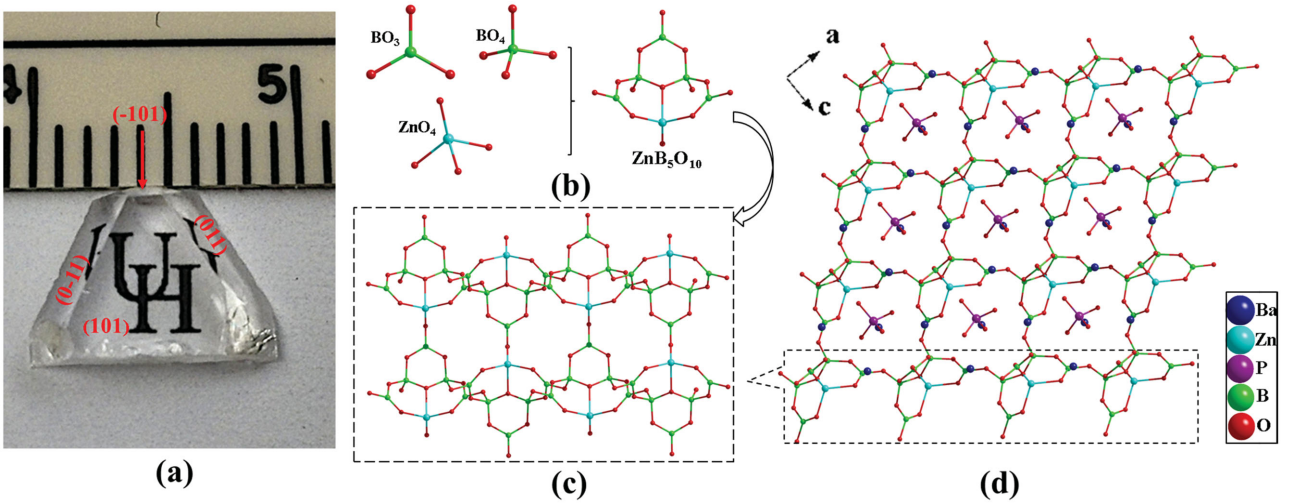

Figure 1. Macroscopic and atomic scale structure of $Ba_3(ZnB_5O_{10})PO_4$. a) Photo of a well-faceted $9 \times 7 \times 3$ mm^3 crystal. b)The ZnB_5O_{10} units consist of BO_3, BO_4, and ZnO_4 polyhedra. c) These anionic groups are linked through Zn–O–B bonds to form a network within which the d) PO_4^{2-} anions and Ba^{2+} cations occupy the channels.

Adv. Mater. **2015**,
DOI: 10.1002/adma.201503951

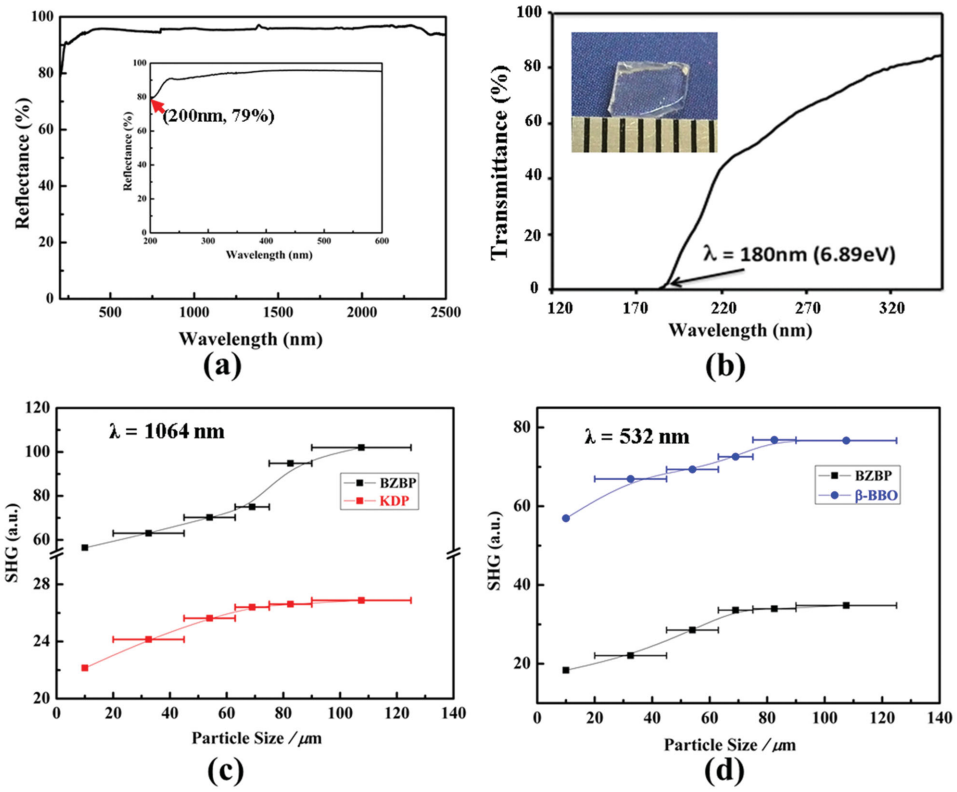

Figure 2. Linear and nonlinear optical properties of $Ba_3(ZnB_5O_{10})PO_4$. a) Diffuse reflection spectrum on polycrystalline BZBP shows that the reflectance is nearly 80% at 200 nm. b) DUV transmission spectrum on single crystal BZBP indicates the absorption edge is at 180 nm. Powder SHG measurements at c) 1064 nm and d) 532 nm reveal that BZBP is type-1 phase-matchable.

532 and 266 nm radiation was detected: The SHG efficiencies as a function of particle size, shown in Figure 2 c,d, indicate that BZBP has SHG efficiencies of approximately 4 × KDP and 0.5 × β-BBO at 532 and 266 nm, respectively, in the 45–63 μm particle range. Furthermore, BZBP is type-1 phase-matchable at both wavelengths.

To better understand the structural and electronic origin of the optical properties in BZBP, we investigated the material using representation theory methods combined with electronic structure calculations based on density functional theory (DFT). First, we performed an analysis of the polar $Pmn2_1$ structure, disentangling the specific atomic displacements that contribute to the loss of inversion symmetry, which is a prerequisite for the NLO response. We identified a theoretical high symmetry, inversion-containing structure for BZBP in space group *Pmnm* (no. 59), and relaxed the internal atomic positions while fixing the lattice parameters to those of the experimental $Pmn2_1$ phase. By performing a symmetry-adapted mode analysis, we identified two displacive modes relating the hypothetical centrosymmetric *Pmnm* phase to the polar structure. The first is an inversion preserving mode that transforms as the irreducible representation (irrep) Γ_1^+ and consists of small O displacements, but retains the *Pmnm* symmetry. The second mode transforms as the Γ_3^- irrep and consists of the following displacements: antipolar Ba displacements, shifts in the Zn and P cations, and rotations of the B–O bond network. The loss of inversion symmetry is attributable to the Γ_3^- mode owing to the rotations of the B–O groups from which the BO_3 triangles result and are characteristic of the $Pmn2_1$ structure (**Figure 3**). Furthermore, these rotations bring O(6) and O(7) closer to the Ba, Zn, and P atoms (Table S2, Supporting Information), and, together with the borate units, are responsible for the formation of the acentric ZnO_4 and PO_4 tetrahedra that comprise the ZnB_5O_{13} group in the $[ZnB_5O_{10}]_\infty$ framework.

We further investigate the role of the polar mode in influencing the NLO response through the electronic structure by computing the atomic and orbital resolved density of states (Figure 3). In the high symmetry *Pmnm* phase (Figure 3a), we find the valence and conduction bands are made up primarily of O 2p states, with Ba 4d states near 3 eV, respectively. Additionally, the filled Zn 3d states are highly localized around –6.5 to –6 eV, while B 2p states are dispersed throughout the valence band. Interestingly, we find in the hypothetical centrosymmetric BZBP phase, there are O 2p and P 3p states in the middle of the band gap centered near 1.5 eV. Upon the addition of the polar Γ_3^- mode, the rotation of the B–O groups fully forms the PO_4 tetrahedra, pushing the formerly mid-gap states down in energy into the valence band and allowing the Ba 4d states to form the conduction band (Figure 3b). Additionally, these oxygen displacements (rotations) give rise to the ZnO_4 tetrahedra; accordingly, the increased hybridization with the O 2p states shifts the Zn 3d bands to become higher in energy and more dispersive.

Finally, in the experimental structure consisting of both the Γ_1^+ and Γ_3^- (Figure 3c), we find the electronic band gap

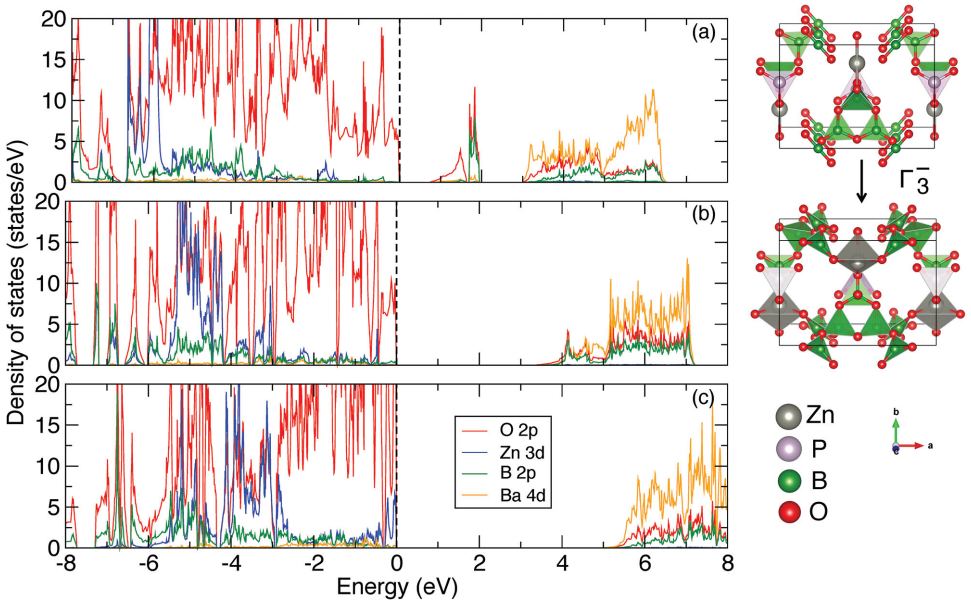

Figure 3. Electronic structure and acentric mode producing polar $Ba_3(ZnB_5O_{10})PO_4$. a) The atomic and orbital resolved density of states (DOS) for BZBP in the centrosymmetric *Pmnm* reference geometry ($\Gamma_1^+ = \Gamma_3^- = 0$ Å mode amplitude). b) DOS of the polar structure with the Γ_3^- mode at the equilibrium value found in the experimental structure ($\Gamma_1^+ = 0$ Å) and c) DOS for the experimental $Pmn2_1$ ground state. The atomic displacements corresponding to the Γ_3^- mode, resulting in the formation of BO_3 triangles, and ZnO_4 and PO_4 tetrahedra, are shown to the right (Ba atoms are omitted for clarity). Note that the small oxygen displacements described by the Γ_1^+ mode then capture the differences in features between panels (b) and (c). The dashed line at 0 eV indicates the Fermi level.

computed at the PBEsol density functional theory level is 4.84 eV, smaller than the experimental value and consistent with the known underestimation of the band gap within DFT. The valence band consists primarily of O 2p and Zn 3d states near the Fermi level (0 eV), with strong overlap with the O 2p, Zn 3d, and B 2p states from –6 to –3 eV. These electronic structure features are consistent with the fact that the primary crystal structural units forming BZBP are the functional $[ZnB_5O_{13}]$ building units. The rotation of the B–O groups characterized by the Γ_3^- mode therefore is pivotal for enabling the SHG because it redistributes charge by the formation of the B–O–Zn bond and ZnO_4 tetrahedra. It allows for a sharp onset of the valence and conduction band edges across which virtual excitations occur for SHG. The mode and active units permit the wide optical transparency needed for frequency conversion in the DUV. In particular, the valence band maximum consists of Zn 3d states of O 2p states derived from the ZnO_4 tetrahedra. These orbitals comprise a portion of the $[ZnB_5O_{13}]$ unit and along with the BO_3 triangles make the most important contributions to the NLO response. The extended transparency range is made possible by the conduction band which consists of Ba 4d states and the formation of PO_4 anionic groups as described above.

Based on these electronic structures, we next calculated the linear refractive index, which indicates a birefringence of $\Delta n = 0.035$ at 532 nm at the PBEsol level ($\Delta n = 0.040$ at the experimental gap, obtained using the scissor correction.). This value is comparable, albeit smaller, than other known borates, but nonetheless BZBP can be used for frequency doubling. We then computed the SHG coefficients, d_{ij}, and use them to understand the structure-optical property relationship. The crystal class exhibited by BZBP (*mm*2) allows for five nonzero SHG coefficients, d_{31}, d_{32}, d_{33}, d_{24}, and d_{15}.[28] The largest coefficients of these are $d_{31} = d_{15} = 1.62$ pm V^{-1} (under Kleinman symmetry), which makes the SHG tensor properties of BZBP comparable if not superior to other commercial DUV NLO materials (**Table 1**). Finally, we relate the magnitude of the SHG coefficients to the static crystal structure by quantifying the magnitude or "degree" to which inversion symmetry is lifted using a vector consisting of the normalized atomic displacements relating the high and low symmetry phase of BZBP. By normalizing the amplitude of these distortions by the cell volume, we obtain the so-called "specific-acentric mode displacements," or SAMD; in addition to a measure of the polar distortion, it also allows for comparison across families with different chemistries and crystal structures. For BZBP, we computed a SAMD of 13.3×10^{18} Å cm^{-3}, which is approximately the same as that obtained for KBBF (Table 1), making it a highly attractive, alternative Be-free NLO material for DUV operation.

In summary, we have designed and synthesized a new Be-free NLO crystal $Ba_3(ZnB_5O_{10})PO_4$, which exhibits a DUV absorption edge, large SHG responses, and is type-1 phase-matchable. Importantly, the crystal is stable in both air and water and melts congruently, enabling the facile growth of large single crystals. We showed using ab initio calculations and a mode crystallographic analysis that the nonlinear response originates in the static microscopic distortions present in the acentric crystal structure, specifically from an effective rotation of the B–O bond network which forms the BO_3 triangles and ZnO_4 tetrahedra. Combining this understanding with the judicious use of anionic groups that have the targeted electronic-optical features has enabled us to discover an NLO material with superior properties operating in the elusive DUV. The

Adv. Mater. **2015**,
DOI: 10.1002/adma.201503951

Table 1. Optical and structural properties for NLO crystals operating in the DUV. Comparison of the absorption edges, SHG coefficients, and structural descriptor (SAMD) for inversion symmetry breaking reveals that the borate–phosphate $Ba_3(ZnB_5O_{10})PO_4$ reported here (*) is an excellent NLO material.

Material	Absorption edge	SHG coefficients [pm V^{-1}]	SAMD [$\times 10^{18}$ Å cm^{-3}]
$KBe_2BO_3F_2$ (KBBF)[4,29]	147 nm (8.43 eV)[9]	$d_{11} = 0.47 \pm 0.01$[9]	13.8
LiB_3O_5 (LBO)[9,29]	155 nm (8 eV)[29]	$d_{31} = \pm 0.83$ (± 0.67)[29]	–
		$d_{32} = \pm 0.89$ (± 0.85)[29]	
		$d_{33} = \pm 0.05$ (± 0.04)[29]	
$Sr_2Be_2B_2O_7$ (SBBO)[10,29]	155 nm (8 eV)[29]	$d_{22} = 2.0$–2.48[10]	–
CsB_3O_5 (CBO)[9,29]	167 nm (7.42 eV)[29]	$d_{14} = 0.75$[29]	–
$NaSr_3Be_3B_3O_9F_4$ (NSBBF[11]	170 nm (7.29 eV)[11]	$d_{11} = -d_{21} = 1.32$[a)][11]	10.4
		$d_{33} = -0.52$[a)][9]	
$CsLiB_6O_{10}$ (CLBO)[9,29]	180 nm (6.89 eV)[29]	$d_{36} = 0.95$ (0.74) [29]	–
$K_3B_6O_{10}Cl$ (KBOC) [30,31]	180 nm (6.89 eV)[30]	–	8.73
$Ba_3(ZnB_5O_{10})PO_4$ (BZBP)*	180 nm (6.89 eV)	$d_{31} = d_{15} = 1.62$[b)]	13.3
		$d_{32} = d_{24} = -0.634$[b)]	
		$d_{33} = -0.540$[b)]	
β-BaB_2O_4 (β-BBO[9,29]	185 nm (6.70 eV)[29]	$d_{22} = 1.60 \pm 0.05$[29]	–
		$d_{22} = 2.20 \pm 0.051$[32]	
$Li_4Sr(BO_3)_2$[33]	186 nm (6.67 eV)[33]	$d_{11} = -0.71$[a)][33]	15.1
		$d_{12} = 0.64$[a)][33]	

– = Not reported.
[a)]Estimated from powder SHG data; [b)]Calculated in the static limit ($\hbar\omega = 0$).

methodology may be expanded to discover new functional materials with linear and nonlinear properties at other important regions of the electromagnetic spectrum.

Experimental Section

Synthesis: Polycrystalline BZBP was synthesized by conventional solid-state methods. Stoichiometric amounts of $BaCO_3$ (Fisher Scientific, 99%), ZnO (Assay, 99.0%), H_3BO_3 (Alfa Aesar, 99.0%), and $NH_4H_2PO_4$ (Alfa Aesar, 98.0%) were ground thoroughly, packed tightly in a platinum crucible, and heated to 400 °C for 20 h, to decompose $NH_4H_2PO_4$ and H_3BO_3. The temperature was raised to 840 °C, held for 72 h, with several intermittent grindings. Laboratory powder X-ray diffraction indicated pure BZBP was obtained (Figure S1, Supporting Information).

Crystal Growth: A single crystal of BZBP was grown by the top seeded solution growth method. Polycrystalline BZBP was mixed thoroughly with H_3BO_3 and ZnO at a molar ratio of BZBP:H_3BO_3:ZnO = 1:3.5:0.7. The mixture was heated to 980 °C in a platinum crucible, to create a melt, in a vertical and programmable temperature furnace. This temperature was held for 15 h in order for the melt to be clear and homogeneous. A platinum wire was then dipped into the melt. The temperature was decreased to 840 °C at a rate of 2 °C h^{-1}. Some small crystals were observed to nucleate on the platinum wire. Then the platinum wire was pulled out of the solution, and allowed to cool to room temperature at a rate of 10 °C h^{-1}. These small crystals were used as seeds for the larger single crystal growth. The seed crystal was dipped into the melt following the procedure described above (Figure S5, Supporting Information).

Structural Characterization: Powder X-ray diffraction analysis was carried out at room temperature on a PANalytical X'Pert PRO diffractometer equipped with Cu Kα radiation. Single-crystal X-ray diffraction data were collected on a Bruker SMART APEX2 diffractometer equipped with a 4K CCD area detector using graphite-monochromated Mo Kα radiation. Data were integrated using the Bruker SAINT program,[34] with the intensities corrected for Lorentz factor, polarization, air absorption, and absorption attributable to the variation in the path length through the detector faceplate. Absorption corrections based on the multiscan technique were also applied. The structure was solved by direct methods using SHELXS-97.[35] All atoms were refined using full matrix least-squares techniques, final least-squares refinement is on F_o^2 with data having $F_o^2 \geq 2\sigma(F_o^2)$. The structure was verified using the ADDSYM algorithm from the program PLATON[36] and no higher symmetries were found.

Physical Property Measurements: The IR spectrum was recorded with a Bruker Tensor 37 Fourier transform infrared (FTIR) spectrometer in the 400–4000 cm^{-1} range using KBr pellets (Figure S4, Supporting Information). The main IR absorption region between 1458 and 507 cm^{-1} reveals several absorption bands attributable to stretching and bending vibrations of the B–O and P–O groups, which are consistent to those of other borate-phosphates.[18–20]

The UV–vis–NIR diffuse reflectance spectrum was measured at room temperature with a Cary 5000 UV–vis–NIR spectrophotometer in the 200–2500 nm wavelength range. DUV absorption measurements from 120 to 200 nm were performed on a VUVas2000 (McPherson). A single crystal with a thickness of ≈1 mm was cut from a grown crystal (Figure 2b, inset).

The thermal properties were measured on EXSTAR TG/DTA 6300 instrument under flowing nitrogen gas, heated from room temperature to 1000 °C at a rate of 5 °C min^{-1} (Figure S2, Supporting Information). Powder SHG were measured by using the Kurtz–Perry method with Q-switched Nd:YAG lasers at 1064 and 532 nm, i.e., SHG was measured at 532 and 266 nm.[37] Polycrystalline samples of BZBP, KDP, and β-BBO were ground and sieved into distinct particle size ranges (<20, 20–45, 45–63, 63–75, 75–90, 90–120, >120 μm). The sieved KDP and β-BBO powders were used as a reference at 1064 and 532 nm respectively. The intensity of the frequency-doubled output emitted from the sample was measured using a photomultiplier tube.

Computational Methods: The structural relaxation of the high symmetry phase, density of states, and linear optical calculations were

performed using density functional theory[38] as implemented in the Vienna ab initio simulation package (VASP).[39,40] We used projector augmented-wave (PAW) potentials[41] with the PBEsol functional.[42] The following valence electron configurations were used for the PAWs: $5s^25p^66s^2$ for Ba, $3d^{10}4s^2$ for Zn, $3s^23p^3$ for P, $2s^23p^1$ for B, and $2s^22p^4$ for O. We obtained the hypothetical high symmetry *Pmnm* aided by the PSEUDO tool of the Bilbao crystallographic server,[43] and relaxed the internal atomic positions using a 650 eV plane wave cutoff and $5 \times 5 \times 5$ Monkhorst-Pack *k*-point mesh.[44] We then performed a symmetry adapted mode decomposition using the ISODISTORT tool of the ISOTROPY suite.[45] The density of states of each phase was computed using a 650 eV plane wave cutoff and $9 \times 9 \times 9$ *k*-point mesh. To obtain the refractive index and birefringence, we computed the frequency dependent dielectric tensor using a 650 eV plane wave cutoff and $5 \times 5 \times 5$ *k*-point mesh, including 1870 empty bands in the calculation. We computed the nonlinear optical properties using density functional perturbation theory (within the local density approximation, LDA) as implemented in ABINIT[46] with a 650 eV plane wave cut off and $5 \times 5 \times 5$ *k*-point mesh. Norm-conserving pseudopotentials were generated using the Troullier–Martins scheme. The following valence electron configurations were used: $5p^66s^2$ for Ba, $3d^{10}4s^2$ for Zn, $3s^23p^3$ for P, $2s^23p^1$ for B, and $2s^22p^4$ for O.

Further details of the crystal structure investigation may be obtained from the Fachinformationszentrum Karlsruhe, D-76344 Eggenstein-Leopoldshafen (Germany), on quoting the depository number CSD-430062.

Supporting Information

Supporting Information is available from the Wiley Online Library or from the author.

Acknowledgements

H.Y., W.Z., and P.S.H. thank the Welch Foundation (Grant No. E-1457) and NSF DMR-1503573 for support. J.Y. and J.M.R. were supported by the National Science Foundation under Grant No. DMR-1454688. Calculations were performed on the CARBON cluster at the Center for Nanoscale Materials [Argonne National Laboratory, supported by the U.S. DOE, Office of Basic Energy Sciences (BES), DE-AC02-06CH11357] under allocation CNM39812. J.Y. thanks Dr. A. Cammarata for useful discussions.

Received: August 13, 2015
Revised: September 2, 2015
Published online:

[1] P. Becker, *Adv. Mater.* **1998**, *10*, 979.
[2] P. S. Halasyamani, K. R. Poeppelmeier, *Chem. Mater.* **1998**, *10*, 2753.
[3] Y. Mori, Y. K. Yap, T. Kamimura, M. Yoshimura, T. Sasaki, *Opt. Mater.* **2002**, *19*, 1.
[4] C. Chen, G. Wang, X. Wang, Z. Xu, *Appl. Phys. B* **2009**, *97*, 9.
[5] X. Jiang, L. Kang, S. Luo, P. Gong, M.-H. Lee, Z. Lin, *Int. J. Mod. Phys. B* **2014**, *28*, 1430018.
[6] W. Yao, R. He, X. Wang, Z. Lin, C. Chen, *Adv. Opt. Mater.* **2014**, *2*, 411.
[7] X. Jiang, S. Luo, L. Kang, P. Gong, H. Huang, S. Wang, Z. Lin, C. Chen, *ACS Photon.* **2015**, *2*, 1183.
[8] I. Chung, M. G. Kanatzidis, *Chem. Mater.* **2014**, *26*, 849.
[9] C. T. Chen, R. K. Li, Y. Wu, Z. Lin, Y. Mori, Z. Hu, J. Wang, S. Uda, M. Yoshimura, Y. Kaneda, *Nonlinear Optical Borate Crystals*, Wiley-VCH, Weinheim, Germany **2012**.
[10] C. T. Chen, Y. B. Wang, B. C. Wu, K. C. Wu, W. L. Zeng, L. H. Yu, *Nature* **1995**, *373*, 322.
[11] H. Huang, J. Yao, Z. Lin, X. Wang, R. He, W. Yao, N. Zhai, C. Chen, *Angew. Chem. Int. Ed.* **2011**, *50*, 9141.
[12] S. Wang, N. Ye, *J. Am. Chem. Soc.* **2011**, *133*, 11458.
[13] S. Wang, N. Ye, W. Li, D. Zhao, *J. Am. Chem. Soc.* **2010**, *132*, 8779.
[14] P. Yu, L. M. Wu, L. J. Zhou, L. Chen, *J. Am. Chem. Soc.* **2013**, *136*, 480.
[15] S. Zhao, P. Gong, S. Luo, L. Bai, Z. Lin, C. Ji, T. Chen, M. Hong, J. Luo, *J. Am. Chem. Soc.* **2014**, *136*, 8560.
[16] S. Zhao, P. Gong, S. Luo, L. Bai, Z. Lin, Y. Tang, Y. Zhou, M. Hong, J. Luo, *Angew. Chem. Int. Ed.* **2015**, *27*, 4291.
[17] T. Sun, P. Shan, H. Chen, X. Liu, H. Liu, S. Chen, Y. A. Cao, Y. Kong, J. Xu, *CrystEngComm* **2014**, *16*, 10497.
[18] X. Zhang, L. Wang, S. Zhang, G. Wang, S. Zhao, Y. Zhu, Y. Wu, C. Chen, *J. Opt. Soc. Am. B-Opt. Phys.* **2011**, *28*, 2236.
[19] B. Ewald, Y. X. Huang, R. Kniep, *Z. Anorg. Allg. Chem.* **2007**, *633*, 1517.
[20] Y. Wang, S. Pan, S. Huang, L. Dong, M. Zhang, S. Han, X. Wang, *D. Trans.* **2014**, *43*, 12886.
[21] S. Huang, H. Yu, J. Han, S. Pan, Q. Jing, Y. Wang, L. Dong, H. Wu, Z. Yang, X. Wang, *Eur. J. Inorg. Chem.* **2014**, *2014*, 3467.
[22] C. T. Chen, Y. C. Wu, R. K. Li, *Int. Rev. Phys. Chem.* **1989**, *8*, 65.
[23] H. Yu, H. Wu, S. Pan, Z. Yang, X. Hou, X. Su, Q. Jing, K. R. Poeppelmeier, J. M. Rondinelli, *J. Am. Chem. Soc.* **2014**, *136*, 1264.
[24] H. Wu, S. Pan, H. Yu, Z. Chen, F. Zhang, *Solid State Sci.* **2012**, *14*, 936.
[25] S. L. Pan, Y. C. Wu, P. Z. Fu, X. Wang, G. C. Zhang, C. T. Chen, *J. Opt. Soc. Am. B-Opt. Phys.* **2004**, *21*, 761.
[26] I. D. Brown, D. Altermatt, *Acta Crystallogr. Sect. B-Struct. Sci.* **1985**, *41*, 244.
[27] K. M. Ok, E. O. Chi, P. S. Halasyamani, *Chem. Soc. Rev.* **2006**, *35*, 710.
[28] S. N. Rashkeev, W. R. L. Lambrecht, B. Segall, *Phys. Rev. B* **1998**, *57*, 3905.
[29] V. G. G. Dmitriev, D. N. Nikogosyan, *Handbook of Nonlinear Optical Crystals*, Springer, New York **1995**.
[30] H. Wu, S. Pan, K. R. Poeppelmeier, H. Li, D. Jia, Z. Chen, X. Fan, Y. Yang, J. M. Rondinelli, H. Luo, *J. Am. Chem. Soc.* **2011**, *133*, 7786.
[31] H. Wu, S. Pan, H. Yu, D. Jia, A. Chang, H. Li, F. Zhang, X. Huang, *CrystEngComm* **2012**, *14*, 799.
[32] R. C. Eckardt, H. Masuda, Y. X. Fan, R. L. Byer, *IEEE J. Quantum Electron.* **1990**, *26*, 922.
[33] S. G. Zhao, P. F. Gong, L. Bai, X. Xu, S. Q. Zhang, Z. H. Sun, Z. S. Lin, M. C. Hong, C. T. Chen, J. H. Luo, *Nat. Commun.* **2014**, *5*, 1.
[34] Bruker, *SAINT*. Bruker AXS Inc., Madison, WI **2007**.
[35] G. M. Sheldrick, *Acta Crystallogr. A* **2008**, *64*, 112.
[36] A. L. Spek, *J. Appl. Crystallogr.* **2003**, *36*, 7.
[37] S. K. Kurtz, T. T. Perry, *J. Appl. Phys.* **1968**, *39*, 3798.
[38] P. Hohenberg, W. Kohn, *Phys. Rev. B* **1964**, *136*, 864.
[39] G. Kresse, J. Hafner, *Phys. Rev. B* **1993**, *47*, 558.
[40] G. Kresse, J. Furthmuller, *Comput. Mater. Sci.* **1996**, *6*, 15.
[41] P. E. Blöchl, *Phys. Rev. B* **1994**, *50*, 17953.
[42] J. P. Perdew, A. Ruzsinszky, G. I. Csonka, O. A. Vydrov, G. E. Scuseria, L. A. Constantin, X. Zhou, K. Burke, *Phys. Rev. Lett.* **2008**, *100*, 136406.
[43] E. Kroumova, M. I. Aroyo, J. M. Perez-Mato, S. Ivantchev, J. M. Igartua, H. Wondratschek, *J. Appl. Crystallogr.* **2001**, *34*, 783.
[44] H. J. Monkhorst, J. D. Pack, *Phys. Rev. B* **1976**, *13*, 5188.
[45] B. J. Campbell, H. T. Stokes, D. E. Tanner, D. M. Hatch, *J. Appl. Crystallogr.* **2006**, *39*, 607.
[46] X. Gonze, B. Amadon, P. M. Anglade, J. M. Beuken, F. Bottin, P. Boulanger, F. Bruneval, D. Caliste, R. Caracas, M. Côté, T. Deutsch, L. Genovese, P. Ghosez, M. Giantomassi, S. Goedecker, D. R. Hamann, P. Hermet, F. Jollet, G. Jomard, S. Leroux, M. Mancini, S. Mazevet, M. J. T. Oliveira, G. Onida, Y. Pouillon, T. Rangel, G. M. Rignanese, D. Sangalli, R. Shaltaf, M. Torrent, M. J. Verstraete, G. Zerah, J. W. Zwanziger, *Comput. Phys. Commun.* **2009**, *180*, 2582